



Impact of metakaolin on mechanical performance of flax textile-reinforced cement-based composites

Filip Majstorović^{a,*}, Vaclav Sebera^{a,b}, Maruša Mrak^c, Sabina Dolenc^c, Marco Wolf^d, Laetitia Marrot^{a,e}

^a InnoRenew CoE, Livade 6, 6310, Izola, Slovenia

^b Department of Wood Science and Technology, Mendel University in Brno, Zemědělská 1, Brno, 61300, Czech Republic

^c Slovenian National Building and Civil Engineering Institute, Dimičeva ulica 12, 1000, Ljubljana, Slovenia

^d Center for Light and Environmentally-Friendly Structures ZELUBA®, Fraunhofer Institute for Wood Research, Wilhelm-Klauditz-Institut WKI, Bienroder Weg 54E, 38108, Braunschweig, Germany

^e University of Primorska, Andrej Marušič Institute, Muzejski trg 2, 6000, Koper, Slovenia

ARTICLE INFO

Keywords:

Textile-reinforced concrete (TRC)
Flax textile
Natural fibres
Finite element
Metakaolin
Cement-based composites

ABSTRACT

This study presents research on the effect of Portland cement (PC) replacement with metakaolin on the mechanical behavior of flax textile-reinforced cementitious matrices (TRCM). The composition of cementitious matrices and in-situ flax fibres was determined using X-ray diffraction and thermogravimetric analysis, while the reinforcement efficiency of the textile and mechanical behavior of TRCMs was investigated by three-point bending tests and finite element analysis. High amounts of PC replacement with metakaolin provided a calcium hydroxide-free environment, more suitable for the natural fibres, to avoid their degradation and embrittlement and, thus, significantly contribute to the ductility of the cement-based composite material.

1. Introduction

The United Nations established seventeen Sustainable Development Goals (SDG) in 2015, amongst which the 12th goal was “to ensure sustainable consumption and production patterns”. According to the International Energy Agency, achieving the SDG12 while producing enough cement to meet future global demands will depend on reducing the clinker-to-cement ratio and development of innovative technologies [1]. Therefore, improving material efficiency will be one of the key strategies to reduce the total demand for cement and the amount of clinker used for its production. Innovative cement-based composite materials are being developed to meet complex specifications (e.g., tensile, flexural and impact properties), and science has turned to find ways of introducing new materials that offer sustainability and renewability in addition to the required mechanical performance. Specifically, natural fibres are attracting attention from the scientific community as materials to reinforce cement-based composites [2–4] due to their wide availability at relatively low cost, renewability, biodegradability and desirable physical and mechanical properties [5–8].

Natural fibres can be randomly dispersed in the cementitious matrix, aligned in the form of long fibres/rovings, or woven as a textile structure before being introduced into the matrix [9–12]. When dispersed, due to the fibres’ random distribution and varying properties (i.e., chemical composition, dimensions and surface roughness), their strength cannot be fully utilized. Hence, this form of reinforcement usually requires a larger volume of fibres, which leads to workability issues associated with high fibre content present in the mixture [13,14]. Within a textile, a high number of fibres are involved, which provides a levelling effect of their fluctuating individual mechanical properties. Moreover, the arrangement of the fibres in twisted yarns bring additional friction between the fibres, contributing to the homogenization of the textile reinforcement properties, and allows the fibres to be aligned in the orientation of developed stresses, resulting in strain-hardening behavior that gives cement-based composites high strength and ductility [15]. Furthermore, the geometry of the textile (e.g., weave) contributes to an enhanced fibre-matrix interface bonding by improving mechanical anchorage of the textile fibres with the cementitious matrix [16,17].

Literature reports the mechanical performance of various natural

Abbreviation: CH, Calcium hydroxide; C–S–H, Calcium silicate hydrate; MK, Metakaolin; PC, Portland cement; TRCM, Textile-reinforced cementitious matrix..

* Corresponding author.

E-mail addresses: filipmajstorovic5@gmail.com (F. Majstorović), vaclav.sebera@innorenew.eu (V. Sebera), marusa.borstnar@zag.si (M. Mrak), sabina.dolenc@zag.si (S. Dolenc), marcowolf1501@gmail.com (M. Wolf), laetitia.marrot@innorenew.eu (L. Marrot).

<https://doi.org/10.1016/j.cemconcomp.2021.104367>

Received 28 May 2021; Received in revised form 13 November 2021; Accepted 29 November 2021

Available online 1 December 2021

0958-9465/© 2021 The Authors. Published by Elsevier Ltd. This is an open access article under the CC BY license (<http://creativecommons.org/licenses/by/4.0/>).

fibre textile-reinforced cementitious matrices (TRCM), such as flax [10, 18–22], sisal [10,18,22], jute [19,23], hemp [22,24], cotton [22,25] and curaua TRCM [26]. The above-mentioned experimental studies present promising mechanical behavior of natural fibre textiles, with flax fibres showing the greatest potential for strengthening applications. Indeed, flax fibres display high specific mechanical properties when compared to other natural fibres [27], and their specific mechanical performances, most notably their stiffness, are comparable to the ones of synthetic E-glass fibres [28]. However, literature concurrently emphasizes several mechanical drawbacks linked to the significant deformability of the textile, causing progressive fibre rupture due to non-uniform deformations at low strain levels [29], and the need of impregnation treatments to obtain more reliable strain hardening composites. The mechanical performance of hybrid textile-reinforced mortar composites comprised of low amount of dispersed fibres and impregnated flax textile reinforcement has been reported [30], addressing above mentioned issues regarding matrix workability and inconsistent fibre deformation. The dispersed fibres allowed to reduce the mean crack width and the hybrid configuration presented an increase of dissipated energy with respect to the conventional flax TRCMs. Beside the particular mechanical behavior of natural fibres, there is still a lack of adequate understanding when it comes to their durability within the alkaline environment of cementitious matrices, which currently limits their potential application as a reinforcement material in cement-based materials. The highly alkaline environment of the cementitious matrix is a consequence of cement hydration, which is initiated when Portland cement (PC) and water are mixed. The hydration process results in the formation of new compounds, most notably calcium silicate hydrate ($\text{CaH}_2\text{O}_4\text{Si}$) and calcium hydroxide ($\text{Ca}(\text{OH})_2$), more commonly referred to as C–S–H and CH in cement chemistry. While C–S–Hs contribute to the strength and durability of the material, CH, which is dissolved in the water of matrix pores and constitutes ~15% of completely hydrated cement paste, is responsible for maintaining a highly alkaline environment (pH 12.5–13) [31]. High alkalinity is harmful to natural fibres as it degrades their components. More specifically, hemicellulose, lignin and pectins within the fibre middle lamella, which is responsible for bonding individual fibre cells together, can be dissolved by alkaline pore water, causing decohesion of the fibres. The cellulose, main component of the cell wall in bast fibres, can also be degraded by alkaline hydrolysis, decreasing its degree of polymerization and lowering the fibre tensile strength [32]. Fibre mineralization due to migration of hydration products (mainly CH) to fibre lumens and middle lamella is another possible fibre degradation mechanism, which in turn causes fibre embrittlement [13,33,34]. Natural fibres are also prone to volume changes caused by their hydrophilic nature which can negatively impact their adhesion to the matrix and overall mechanical properties of the composite [35].

In order to address these concerns, efforts have been made to improve the durability of natural fibres. Studies report impregnation of the fibres with blocking and water-repelling agents, reduction of matrix alkalinity and a combination of those approaches [36,37]. The reduction of matrix alkalinity by the implementation of pozzolanic materials (e.g., metakaolin, fly ash, silica fume) has been studied by several authors [3, 34,36–38]. Toledo Filho et al. [37] discovered that replacing a portion of cement with calcined clay led to a substantial decrease in mineralization of sisal fibres by reducing the amount of CH content present in the matrix. Metakaolin (MK) is a pozzolanic material obtained by calcination of kaolinitic clay at temperatures ranging between 500 and 800 °C. MK is a manufactured product whose quality is controlled during the manufacturing process, which offers more stable characteristics when compared to other industrial pozzolans. However, MK's production process is also associated with higher cost and environmental impact, making its current use economically viable only in countries which possess high amounts of clay [39]. Although MK was first used in the 1960s for dam construction, its prospects have not yet been fully tested, and there have only been a limited number of studies regarding its

potential in natural fibre-reinforced cementitious matrices. When introduced into the mixture, MK initiates a pozzolanic reaction, i.e., it reacts with CH and consumes it to produce additional cementitious materials, such as calcium silicate hydrates (C–S–H), calcium-aluminium-silicate hydrates (C-A-S-H) and calcium aluminate hydrates (C-A-H), resulting in increased strength of the cured material and diminution in alkalinity of the reacting environment [40,41]. Due to its high specific surface area, MK also modifies the microstructure of the cementitious matrices by reducing size of the pores and their overall presence in the matrix, which can also enhance an overall compaction between textile reinforcement and the matrix [42]. Lastly, by providing a more optimal environment for natural fibres, and thus increasing their reinforcing efficiency in cement-based composites, using pozzolanic materials does not only reduce the amount of cement needed for development of the matrix, but also has potential to significantly contribute to strength and durability of the material, and therefore to innovative development of sustainable structures by replacing steel and synthetic materials with renewable and environmentally friendly alternatives.

In this study, flax TRCMs were produced using PC matrices and matrices containing 20–40% of MK. Analyses of physical and mechanical properties of the developed matrices were carried out to correlate the MK's influence on their microstructure, CH content and mechanical performance. The flax textile reinforcing capacity was characterized and its degradation in the matrices' alkaline environment was investigated. The mechanical performance of TRCMs was assessed by three-point bending tests and the effect of MK addition on the fibre-matrix interface bond, failure mechanisms and post-cracking ductility of the TRCM was studied. Furthermore, numerical analysis of TRCMs behavior was carried out using the finite elements (FE) to explore the possibility of predicting their global mechanical response.

2. Materials and methods

2.1. Production, chemical and physical analysis of the cementitious matrices

Within this study, the production of cementitious matrices considered mix designs with 20%, 30% and 40% MK to cement weight ratios (see Table 1). For each mix design, 5 unreinforced and 5 textile reinforced samples were produced. The unreinforced reference samples and the textile-reinforced samples are respectively referred to as control and TRCM samples. However, due to the decrease in matrix workability for higher MK content, caused by its high specific surface and reactivity [43], manufacturing TRCM samples with 40% MK proved too difficult without having to modify the rest of the mixture. Therefore, only control samples with 40% MK were manufactured to examine MK's influence on their physical and mechanical properties.

The fine aggregate used for the mixture was limestone, from Gradbeni materiali d.o.o., with a 0–1 mm grain size and a density of 2.80 g/cm³. Backstein® MK with a particle size of ~2 µm and specific surface area of 14.2 m²/g, and Portland composite cement with limestone and siliceous fly ash (PC) CEM II/B-M (LL-V), purchased from Salanit Anhovo d.d., with a minimum compressive strength of 42.5 MPa at 28

Table 1
Mix designs of the cementitious matrices.

	Binder (PC/ MK) (%)	Aggregate (%)	Superplasticizer/ Binder (%)	Water/ Binder (%)
PC	37.50/0.00	62.5	0.5	46.5
20% MK	30.00/7.50	62.5	1.0	46.5
30% MK	26.25/11.25	62.5	1.3	46.5
40% MK	22.50/15.00	62.5	1.6	46.5

days and a specific surface area of 1.70 m²/g, were used as binders in the mixture. This type of PC already contains pozzolans (i.e., siliceous fly ash) as well as limestone, which together constitute 21–35% of total PC weight, and thus further contribute to a decrease of matrix alkalinity by reducing CH and overall clinker content. Polycarboxylate ether superplasticizer “Viscocrete-2800 Perfin”, obtained from Sika Slovenija d.o.o., was used to compensate for MK’s negative effect on the workability of fresh matrices. The percentage of superplasticizer used in the mixture is directly connected with the amount of binder, and is reported in Table 1.

Porosity of the control samples was determined as an average of 3 measurements performed on one sample for each mixture design using Ultrapyc 5000 gas pycnometer (Anton Paar GmbH, Austria), which continuously measured solid volume of the samples under nitrogen atmosphere and temperature of 25 °C, until variance percentage of less than 0.1% was obtained. The density of each control sample was determined by its mass to volume ratio. Determination of porosity (*P*) and density (*ρ*) of control samples can be seen from the following equations:

$$P[\%] = \frac{V_T - V_S}{V_T} \quad (1)$$

$$\rho \left[\frac{g}{cm^3} \right] = \frac{m}{V_T} \quad (2)$$

Where, *V_T* and *V_S* stand for total (including pores) and solid volume of the control samples, respectively, while *m* stands for the mass of the samples.

The phase composition of the control samples after 56 days of curing was determined using a PANalytical Empyrean X-ray diffractometer (Malvern Panalytical, Malvern, UK) equipped with CuK α radiation and a PIXcel 1D detector. For each mix design, one control sample was first ground to a particle size of less than 0.063 mm, after which it was backloaded into a circular sample holder with a diameter of 27 mm. The samples were then measured at 45 kV at a current of 40 mA, in the range of 5–75° 2 θ , at a step size of 0.013° with a scan time of 130 s. Analysis of X-ray diffraction (XRD) patterns was conducted using X’Pert High Score Plus diffraction software v. 4.9 from PANalytical, using PAN ICSD v. 3.4 powder diffraction files. The Rietveld refinement method was performed using crystal structures according to Snellings et al. [44].

The thermal stability of the developed control samples was measured using thermogravimetric analysis (TGA) on TA Instruments’ “TGA5500”, where weight loss was plotted against temperature in order to obtain derivative thermogravimetric (DTG) and TGA curves. At 56 days of curing, five control samples from each mixture design containing both binder (PC/MK) and aggregates, were left in a laboratory oven under a temperature of 100 °C for 48 h, after which they were ground to a fine powder, as suggested by Kim et al. [45]. XRD and TGA analyses were performed at 56 days of curing instead of 28 days, along with mechanical testing, due to equipment availability constraints. The extended curing period is not believed to have caused significant variations in chemical composition of the matrices, since MK strengthening effect on cementitious matrices happens within the first 14 days of curing, irrespective to the MK content in the matrix [46,47]. The tests were carried out under a nitrogen atmosphere (25 mL/min) and a heating rate of 10 °C/min until a maximum temperature of 800 °C was reached. The CH (i.e. Ca(OH)₂) decomposition to calcium oxide (CaO) and water (H₂O) occurs under temperatures between 350 and 550 °C [48], and this weight loss, caused by evaporation of water, can be used to calculate the amount of CH content in control samples by knowing that one molecule gram of water (18g) originates from decomposition of one molecule gram of CH (74g) [49].

The chemical reaction of CH decomposition and the equation used for the determination of its content can be seen in equations (3) and (4), respectively.



$$CH[\%] = \left(\frac{M_1 - M_2}{M_0} \right) \times \frac{74}{18} \quad (4)$$

Where *M₁* stands for the mass of the sample at the temperature which corresponds to the beginning of CH decomposition, *M₂* stands for the mass of the sample at the temperature which corresponds to the end of CH decomposition, and *M₀* stands for the initial mass of the sample.

2.2. Chemical and mechanical analysis of the flax yarns and textile

Bi-directional woven textile, FlaxDry BL 200, made from single yarns of flax fibres was purchased from the Eco-Technilin company (France). It is composed of a 2/2 twill weave, which means that two warp liftings alternate with two warp lowerings, as seen in Fig. 1. By conducting a microscopic analysis, the size of the mesh opening of the textile was determined to be ~0.6 mm.

Tensile tests were performed on the flax textile by a Z020 testing machine (Zwick Roell) with a pneumatic sample holder, Type 8497, according to DIN EN ISO 13934-1 (Fig. 2 a). Five textile samples of dimensions 250 mm × 50 mm were tested. The clamping length of the setup was 200 mm, and testing speed was set according to sample elongation, either at 20 mm/min or 100 mm/min for elongations below 8% or between 8 and 75%, respectively.

Tensile tests on the flax textile’s yarns were performed on the same testing machine with yarn-adapted grips to avoid sliding or damaging of the samples, in accordance with the EN ISO 2062 standard (Fig. 2b). Ten tensile repetitions were done on 500 ± 2 mm long yarns at the displacement rate of 500 ± 10 mm/min.

TGA was conducted on flax textile samples, operating the same apparatus as used for TGA of matrix control samples, under a nitrogen atmosphere (25 mL/min), using the heating rate of 10 °C/min until a maximum temperature of 800 °C was achieved. Small textile samples (~1 cm², 5 repetitions) were extracted from the TRCM samples after being in contact with them for 56 days. The textile samples were then conditioned in a climate chamber under the temperature of 20 °C and relative humidity of 65%, after which they were subjected to TGA. DTG and TGA curves were analysed and used to investigate the influence of CH content on the degradation of flax textile components i.e., cellulose, hemicellulose and lignin.



Fig. 1. 2/2 twill weave flax textile.

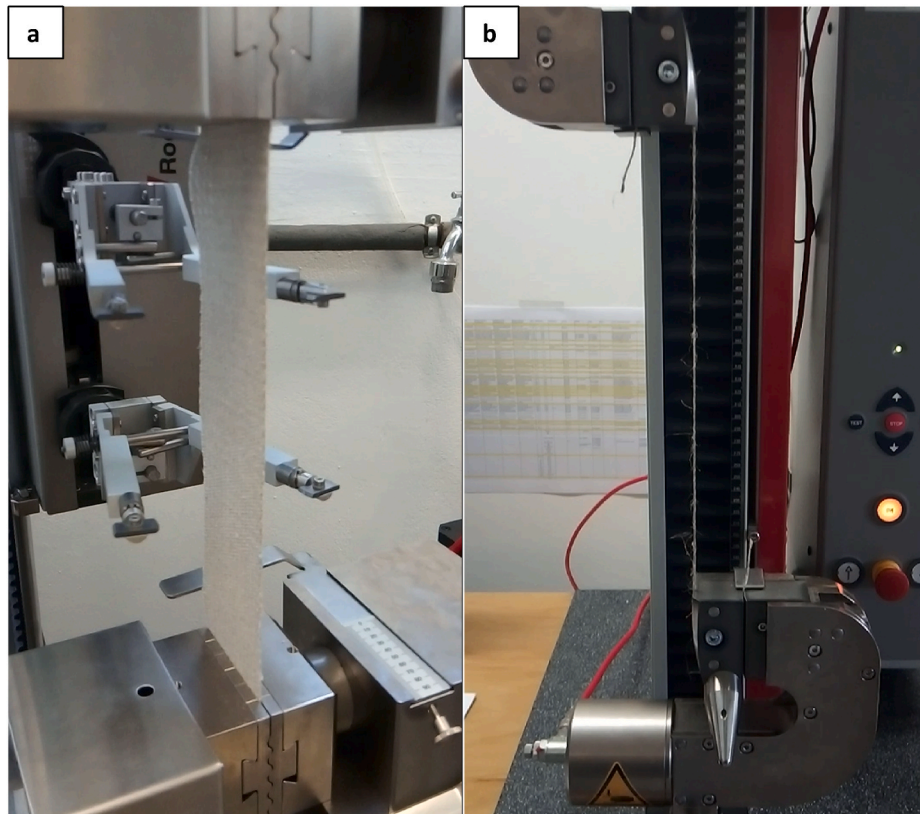


Fig. 2. Tensile test setup for a) flax textile and b) flax yarn.

2.3. TRCM preparation

Prior to the manufacturing process, textile samples were immersed underwater for 1 h to prevent the absorption of the water further introduced for the hydration reaction. After immersion, textile samples were then pressed with a 10 kg steel plate for 10 min to reduce the variations in textile thickness linked to the crimp. The mixing of matrix components was done in three steps. First, the sand and binder were dry mixed for 2 min, after which the water was added and mixed for another 2 min. Finally, superplasticizer was added, and the mixing continued until the desirable matrix consistency was obtained.

An openable wooden custom mould was used to manufacture the samples ($160 \times 40 \times 40 \text{ mm}^3$) (Fig. 3). One batch of 10 samples was produced for each matrix composition. Of those samples, one-half was comprised of non-reinforced cementitious matrices (5 control samples),

and the other half was reinforced with 12 layers of flax textile (5 TRCM samples), corresponding to approximately 3.2% of the total sample weight. The sample manufacturing process can be divided as follows: 1) the first matrix layer, 5.5 mm thick, was poured into the mould and a layer of textile, previously cut to fit the sample dimensions, was placed on top; 2) the textile was gently pressed with a thin sheet of plywood to promote better penetration of matrix through the textile mesh, after which a 2 mm matrix layer was poured on top of the textile; 3) another textile layer was placed upon the matrix layer and the previous step was repeated until all 12 textile layers were placed within the sample; 4) the final matrix layer, 5.5 mm thick, was placed on top of the last textile layer. The table, on which the mould was positioned, was gently vibrated throughout the manufacturing process to improve the workability of the matrix and its bond with the textile reinforcement, as well as to help the evacuation of the gas trapped in the sample. Fresh samples



Fig. 3. Openable wooden mould used for manufacture of non-reinforced (control) and textile reinforced cementitious matrices.

were covered with stretchable plastic film to avoid the evaporation of water. The samples were unmolded after 48 h, after which they were immersed underwater for 12 days (23 °C, 100% RH). Once the immersion phase was over, the samples were stored in standard laboratory conditions (23 °C, 50% RH) for another 14 days, followed by mechanical testing at 28 days.

2.4. Mechanical testing of matrix control samples and TRCM

Three-point bending tests were performed on control and TRCM samples using an Universal Testing Machine (ZwickRoell, Croatia) with a 100 kN load cell in accordance with the DIN EN 12390-5 standard. The bending tests were carried out at a load rate of 50 ± 10 N/s and with a span between supports of 100 mm. 5 control and 5 TRCM samples were tested for each mixture design. Flexural deflections were obtained from the machine crosshead displacement. Fig. 4 shows the bending test setup along with all the relevant dimensions and textile positioning within reinforced samples.

The 5 remaining halves of control specimens obtained from the bending tests were further cut into dimensions of $40 \times 40 \times 40$ mm³ and used to perform compression tests at a load rate of 2400 ± 200 N/s.

The first crack stress of TRCM samples was deduced from the force-deflection curves of the bending test, defined as the first sharp deviation from linearity, and the apparent flexural strength was calculated at the end of the crack propagation phase, assuming the ideal linear behavior of the specimen's cross-section (further illustrated in Fig. 8a). Although apparent stress values differ from real stress values due to nonlinearity, heterogeneity and crack depth, apparent stress values are used to compare different composite scenarios.

The first crack stress (FCS) and flexural strength (σ_f) of TRCM were calculated using the following equations:

$$FCS [MPa] = \frac{3F_c L}{2bd^2} \tag{5}$$

$$\sigma_f [MPa] = \frac{3F_e L}{2bd^2} \tag{6}$$

Where, F_c and F_e stand for the force at first crack and force at the end of crack propagation phase [N], L is the span length [mm], b is specimen width [mm] and d is specimen thickness [mm].

Mechanical work, expressing an area under force-deflection curves, was evaluated until crosshead displacement of 7 mm. After this point, the fibre-matrix interface bond of TRCM samples containing MK was no longer effective due to progressive crack widening, which eventually led to fibre rupture, and thus rapid deterioration of samples. The deterioration phase was inconsistent in its intensity and length, which is believed to be caused by minor flaws, such as compaction variations in certain areas of the matrix associated with the hand lay-up production process, and a high number of textile layers within the samples; therefore, it was not taken into account when calculating the mechanical work. All the parameters were further mutually compared for the groups' means using multiple one-way Analysis of Variance (ANOVA) with a level of significance $\alpha = 0.05$. The statistics were performed in

Matlab 2019 (Mathworks Inc.).

A high-resolution digital camera (9 MPx) with a 23 mm lens (Schneider) and VHX-6000 digital microscope (Keyence, USA) were used to capture images during the bending tests and to record fibre-matrix failure mechanisms and interface bond, respectively. The images were used to examine differences in cracking and failure mechanisms between different TRCM compositions. The image acquisition rate of digital cameras was set at 3 images per second.

2.5. Finite element (FE) analysis

In this section, FE models were developed to examine the influence of the textile on the global behavior of samples under three-point bending. For this purpose, only one matrix type was considered (PC matrix without the addition of MK) using a microplane model and the textile was modeled using various approaches (hyperelastic and two linear isotropic models). The contact of the specimen with supports and loading head was replaced by direct application of boundary conditions on nodes along the width: left support – all degrees of freedom were constrained to zero; right support – only displacement in Y-axis direction was constrained to zero; load-displacement in Y-axis was prescribed as $u_y = -0.5$ mm (Fig. 5a). Within FE analysis, two models of the specimen were developed for: (1) the control samples and (2) the TRCMs. To reduce computational expenses, the specimen was modeled with a width of 1 cm (one-quarter of the physical specimen). The FE mesh was created utilizing 3D solid elements. The cementitious matrix was modeled using CPT215 with linear shape function and with an activated extra nonlocal degree of freedom, and the FE mesh of textile reinforcement was built of linear SOLID185. The general size of the finite element was set to 1 mm lengthwise and 0.9 mm widthwise. The textile layer had a size of FE equal to 0.6 mm via its thickness (Fig. 5a). In total, FE mesh had 73 920 elements (57 600 for cementitious matrix, 16 320 for textile reinforcement) and 83 076 nodes, including shared ones, that resulted in a

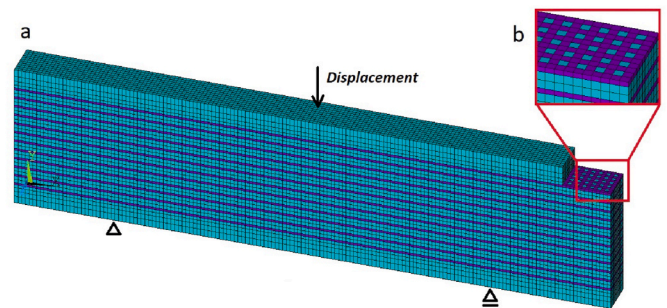


Fig. 5. FE mesh of simulated TRCM specimen with quarter width and sketch of boundary conditions: a) global mesh without corner and b) detail on textile layer. Blue color denotes the cementitious matrix (Microplane), violet color denotes the textile material model. (color online only). (For interpretation of the references to color in this figure legend, the reader is referred to the Web version of this article.)

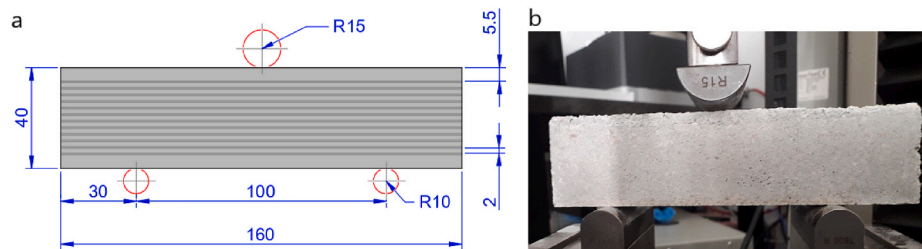


Fig. 4. a) Three-point bending test setup model for non-reinforced (control) matrices and TRCM with 12 textile layers reinforcement b) picture of the test setup with actual sample. (color online only). (For interpretation of the references to color in this figure legend, the reader is referred to the Web version of this article.)

problem of 432 000 equations. The FE sizes were chosen to reduce computational time and by the fact that force/deflection (F/δ) response shows minimal dependency on mesh density when microplane material models are used [50].

Since the textile is porous, the matrix mixture penetrates through it in physical specimens; therefore, matrix is bonded across the textile layers to a certain degree. To model this kind of connection with simplicity, the pores within the textile layer were defined as FEs of the matrix, where they were equally distributed along the layer (Fig. 5b) in the amount of 27%, which is an approximate value taken from image analysis of flax textile. The FE analysis was carried out in Ansys 19 R2 (Ansys Inc., USA) as a nonlinear analysis utilizing an unsymmetrical Newton-Raphson solver.

The material model of matrix control samples utilized the microplane model that is based on the damage approach. Since density and strength in compression of PC matrix were measured at $\rho = 2.11 \text{ g/cm}^3$ and $\sigma_c = 39.1 \text{ MPa}$ respectively, the elastic modulus was obtained using the formula ($E_c = 33 \cdot \rho^{1.5} \cdot \sqrt{\sigma_c}$) provided by the American Concrete Institute [51]. This equation yields $E_{matrix} = 20 \text{ GPa}$. This value was used for all FE simulations. The other parameters for defining the microplane model were taken from Ansys SW (ANSYS Help 2019 R2) and [50]: Poisson's ratio $\mu = 0.18$, damage function parameters $k_0 = k_1 = 0.703125$ and $k_2 = 0.2154553$, damage threshold $\gamma^{mic} = 0.0002$, maximum damage parameter $\alpha^{mic} = 0.96$, rate of damage evolution $\beta^{mic} = 420$, and nonlocal integration range parameter $c = 25e-6$.

We used three types of material models for the textile reinforcement:

- (1) Hyperelastic material using 3-parameter Mooney-Rivlin model derived from the experimental data simplified into six sets of strain/stress points as follows — 0/0, 0.01/0.54e6, 0.02/1.43e6, 0.03/4.32e6, 0.04/14.17e6, and 0.05/30.37e6 (-/Pa); these data were fitted to the 3-parameter Mooney-Rivlin model, which resulted in material parameters of $C10 = -2055827374.3 \text{ Pa}$, $C01 = 2078104212.5 \text{ Pa}$, and $C11 = 12780221183 \text{ Pa}$; calculated residual of the fit was 0.0254;
- (2) Linear isotropic with high elastic modulus (steepest slope from the material test) simulating textile to be pre-stressed ($E = 10.6 \text{ GPa}$ as measured during the experimental textile tensile test);
- (3) Linear isotropic with low elastic modulus (slope from the initial phase of the material test) simulating no pre-stress effect ($E = 600 \text{ MPa}$ as measured during the experimental textile tensile test); for both linear isotropic models, the Poisson's ratio equaled 0.4.

The FE analysis was compared and verified by the experiments based on the F/δ curves for both scenarios (i.e., control samples and TRCM). FE analysis especially focused on a comparison of strength and post-failure load-bearing capacity due to the reinforcement.

3. Results and discussion

3.1. Properties of matrix control samples

Table 2 reports the phase composition of matrix control samples obtained by XRD using the Rietveld refinement technique. For the three matrix types, the presence of residual clinker phases was identified, namely belite, which is a slow hydrating phase, and ferrite, which is detected only in PC where clinker amount is higher in comparison to other mixtures where part of the clinker is substituted with MK. In addition, a small amount of merwinite was noted, which refers to siliceous fly ash in the cement. The amount of merwinite decreased with higher MK content due to a lower proportion of PC in the mixture. Hydrate phases that formed upon hydration were ettringite, hemihydrate and monohydrate, while in PC there was also portlandite (CH) present. Hemihydrate and monohydrate precipitated due to the calcite present in both blended cement and aggregate [45,46].

Table 2

Phase composition of cementitious matrices (in wt. %) obtained by XRD with the Rietveld refinement method.

Cementitious matrix phases	PC	20% MK	30% MK	40% MK
Belite	0.1	0.6	0.5	0.3
Ferrite	0.4	0.0	0.0	0.0
Merwinite	0.2	0.1	0.1	0.0
Ettringite	0.1	0.5	0.6	0.5
Hemihydrate	0.4	0.7	0.7	0.5
Monohydrate	0.7	1.3	1.2	0.5
Portlandite (CH)	2.1	0.0	0.0	0.0
Amorphous	25.1	22.9	22.7	14.9
Calcite	19.9	21.3	20.4	19.2
Dolomite	51.0	52.6	53.8	64.1
SUM	100.0	100.0	100.0	100.0

The siliceous fly ash and limestone constituted between 21 and 35% of total PC weight (data obtained from the provider), resulting in a relatively low content of CH in the matrix due to a lower clinker amount and pozzolanic reaction caused by siliceous fly ash. With the further addition of 20–30% MK, we reached more than 50% PC replacement, and the mixture resulted in a CH-free matrix due to additional clinker replacement and pozzolanic reaction. These CH values are in agreement with the ones reported by Fidelis et al. [52] and Toledo Filho et al. [34], who succeeded in developing a CH-free matrix by replacing 50% of the PC in the mixture with MK and a combination of MK and calcined waste crushed clay brick, respectively. Based on these findings, it can be concluded that depending on the reactivity of the pozzolanic material, total consumption of CH occurs at higher PC replacement levels, specifically 50% and above. The amorphous content is mainly represented by C-(A)-S-H and C-A-H. The amorphous content decreased notably for 40% MK replacement. The amorphous phase is also related to non-reacted MK and fly ash as well as to pore solution. Dolomite and calcite represented a large amount of the composition since they are the main constituents of fine aggregate and blended cement (regarding the calcite).

TGA curves of the control matrix samples for the whole temperature range are presented in Fig. 6a, and TGA and DTG curves of these samples in the temperature range associated with the dehydration of CH are presented, respectively, in Fig. 6b and c. The major weight loss that occurred in the matrices after 600 °C (Fig. 6a) correspond to the decomposition of carbonate minerals, calcite and dolomite, which generally occurs in temperature range between 550 and 850 °C [53–56]. XRD results confirmed a high amount of these phases in the different matrices. The CH content of PC was calculated from the weight loss (Fig. 6b) using the DTG curve peak (Fig. 6c) to identify the temperature range of CH degradation. Hence, between 410 and 480 °C, the CH content was evaluated at 3.0%, which is slightly higher when compared to XRD analysis that reported 2.1%. This higher amount can be explained by the dehydration of less prominent matrix components that happens in the same temperature range. DTG curves of samples containing MK showed no peaks associated with CH dehydration at the time the analysis was performed and confirmed the XRD analysis.

Table 3 shows the mechanical and physical properties of developed cementitious matrices after 28 days of curing. It can be seen that the compressive and flexural strength of the 30% MK samples increased by 25% and 26%, respectively, when compared to PC. This increase in strength was attributed to several factors: (1) the formation of stronger hydration products (such as C-S-H gel and crystalline products) produced by pozzolanic reaction, (2) the fastened and increased consumption of CH due to MK's high reactivity [57], and (3) lower porosity, which was achieved due to finer MK particles that bridged over void spaces between cement particles. A decrease of porosity also correlated to higher densities of the matrices up to 30% MK content. Though the increase in densities was hidden by the lower MK's specific gravity ($\sim 2.60 \text{ g/cm}^3$), when compared to PC ($\sim 3.15 \text{ g/cm}^3$). Wild et al. [47]

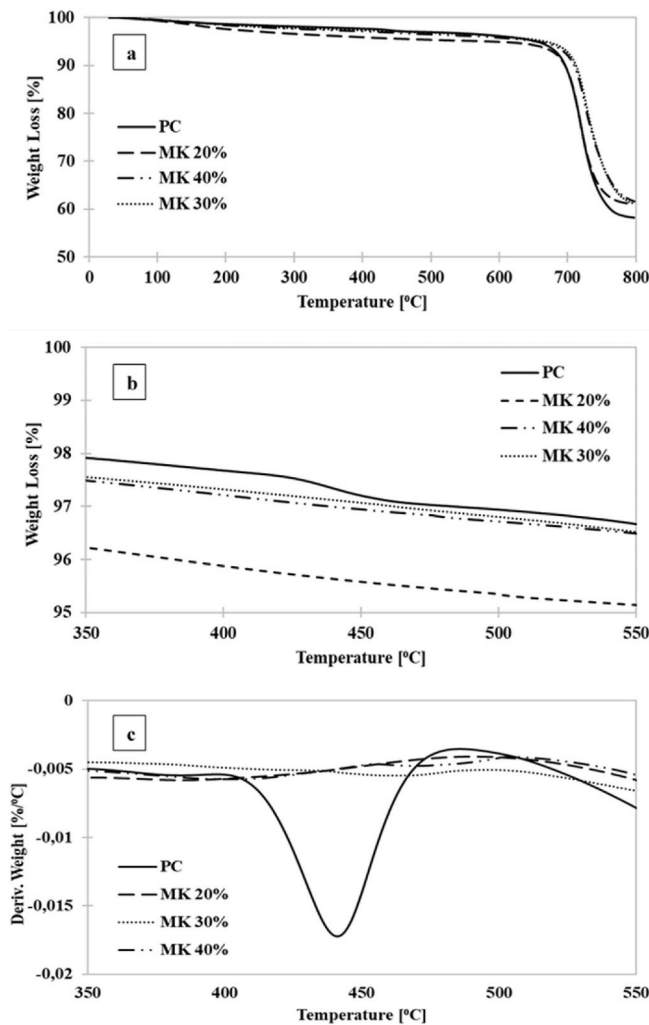


Fig. 6. (a) TGA curve of control matrix samples for the whole temperature range, (b) TGA and (c) DTG curves of control matrix samples in the temperature range associated with CH dehydration.

Table 3

Compressive strength, flexural strength, density and porosity values of cementitious matrices after 28 days of curing (standard variations are in brackets).

	Compressive Strength [MPa]	Flexural strength [MPa]	Density [g/cm ³]	Porosity [%]
PC	39.1 (2.3)	7.6 (0.38)	2.11 (0.026)	18.6 (0.03)
20% MK	47.3 (3.4)	8.3 (0.81)	2.13 (0.038)	10.4 (0.06)
30% MK	49.1 (6.8)	9.6 (0.62)	2.15 (0.021)	8.2 (0.05)
40% MK	47.9 (3.7)	8.8 (0.50)	2.03 (0.026)	17.9 (0.07)

also identified filler effect, acceleration of PC hydration, and the pozzolanic reaction of MK with CH as the three main factors influencing the increase in concrete strength when MK partially replaces cement.

However, at 40% MK content, compressive and flexural strengths as well as density of the matrix decreased, while the porosity increased. This is caused by the clinker dilution effect that happens when a significant amount of cement is replaced by supplementary cementitious materials. This results in reduced content of hydration products present in the matrix (indeed, the amorphous phase determined by XRD in this sample related to the hydration products was the smallest), which

negatively impacts their strength as well as porosity and permeability [58]. The maximum percentage of MK replacement that will have positive effects on the matrix is primarily dependent on the mixture composition (e.g., water to binder ratio, presence of additives) and, thus, it varies among different studies.

3.2. Properties of flax textile reinforcement

Table 4 gathers the characteristics and tensile properties of the flax yarns and textile in the warp and weft directions. When compared to the work of other authors [10,18,19,21,22], flax yarns used for this study had lower linear density (i.e., tex), which correlated to the lower tensile strength of the produced textiles. Therefore, more textile layers were used in TRCM preparation to compensate for its lighter weight and achieve adequate reinforcement (wt %) efficiency. However, Young's modulus and strain to failure values in warp direction were on the higher end when compared to mentioned studies (average values of 3.22–10.1 GPa and 3.7–4.63%, respectively). Better mechanical performance of textile in the warp direction is expected due to higher tension placed on warp fibres, which is keeping them straight during the weaving process, while slightly higher strain to failure in weft direction is explained by more crimp presence in weft yarns, allowing them to handle additional elongation [59].

Fig. 7a and b presents, respectively, TGA and DTG curves of flax textile samples extracted from the TRCM after being in contact with the cementitious matrices for 56 days as well as virgin flax textile (reference). The degradation of the flax fibres can be described in four stages [60]: (1) weight loss from 25 to 150 °C caused by evaporation of water present in the fibres; (2) weight loss from 220 to 315 °C caused by the decomposition of hemicelluloses; (3) weight loss from 315 to 400 °C caused by the decomposition of cellulose; and (4) weight loss after 400 °C due to decomposition of remaining hemicellulose and lignin. Since the degradation of lignin occurs over a broad temperature range, determination of its weight loss using TGA is challenging. However, in the case of flax fibres, lignin degradation can be neglected due to its low amount present in the fibres (1–3%) [27].

No significant difference in water content was observed in the first stage. During stage 2, the reference sample showed higher weight loss caused by the decomposition of hemicelluloses (10.2%) when compared to the fibres that were embedded in the cementitious matrices (~6.4%). However, regardless of the matrix type, there was no significant difference between weight losses of the embedded fibres during this phase, despite the difference in CH content observed in section 3.1 at 56 days of curing for matrices containing PC and MK (CH-free matrices). Indeed, the initial increase of CH content lasts up to seven days after the PC hydration is initiated, after which the CH content starts to decline due to

Table 4

Properties of flax yarn and textile (standard deviations are in brackets).

Flax yarn	Flax textile	Warp/Weft directions
Density [g/cm ³]	1.40	Mesh opening size [mm] 0.6 (0.06)
Tex [g/km]	110	Areal weight [g/m ²] 200
Cross-section [mm ²]	0.079	Cross-section [mm ²] 3.95 ^a
Tenacity [N/Tex]	0.21 (0.04)	Yarn density [No/cm] 10
Tensile strength [MPa]	292.4 (58.5)	Tensile strength [MPa] 249.4 (16.6)/166.3 (18.4)
Strain to failure [%]	1.9 (0.2)	Young's modulus [GPa] 10.6 (0.65)/5.9 (0.36)
		Strain to failure [%] 5.4 (0.3)/5.8 (0.3)

^a Cross-section of textile was calculated as number of yarns present throughout textile width multiplied by yarn cross-section as recommended by Cherif [59].

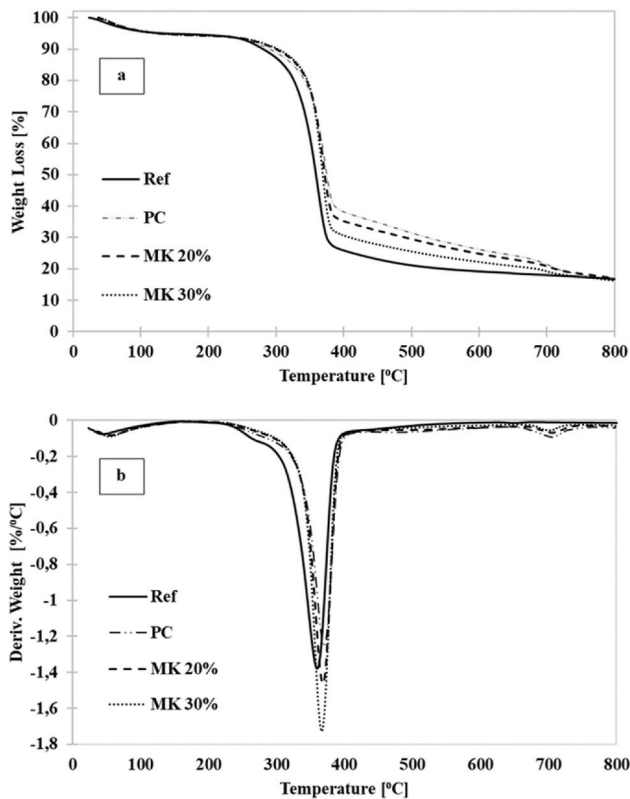


Fig. 7. (a) TGA and (b) DTG curves of flax textile samples extracted from the TRCMs.

the pozzolanic reaction initiated by MK [61]. Due to their location in periphery of the fibre, hemicelluloses from the middle lamella and the primary cell wall are the most accessible and vulnerable to dissolution caused by CH and their decomposition is assumed to occur during this initial hydration stage when CH content of matrices is the highest. Due to the low degree of polymerization of hemicelluloses (50–200), the dominating mechanism behind their decomposition is presumed to be gradual separation of the molecular chain reductive end-groups once they come in contact with hydroxyl groups of CH [32]. Hemicelluloses are responsible for bonding together disordered crystalline cellulose microfibrils in the primary cell wall, and helically ordered crystalline cellulose microfibrils in the secondary cell wall. Degradation of hemicelluloses results in the dispersion of cellulose microfibrils within the matrix pore solution, and facilitates the exposure of cellulose to further degradation. Once components of the middle lamella and primary cell wall undergo degradation, amorphous regions of cellulose microfibrils in the secondary cell wall are more susceptible to alkaline hydrolysis, causing division of molecular chain and exposure of new reductive end-groups which can then be separated. As the degradation proceeds, the hydration products (e.g., C–S–H and CH) are able to breach into the cell wall, causing mineralization and embrittlement of the fibres [62]. Weight losses of cellulose associated with stage 3 were as high as 58.1%, 48.7%, 52.9% and 57.9% for reference, PC, 20% and 30% MK, respectively. Thus, the samples containing MK preserved a higher amount of cellulose during their time embedded in the matrices. The amount of preserved cellulose increased with the percentage of MK in the matrix, where reference and MK 30% samples showed similar cellulose content.

Since similar hemicelluloses degradation was observed in the fibres exposed to different matrices, it can be presumed that fibres decohesion due to damaged middle lamella and primary cell wall occurred in all cases, leading to lower reinforcement capability of the textiles. Textile embedded in matrices containing MK displayed higher preservation of

their cellulose content. Degradation caused by the presence of CH at the first stage of cement hydration was then limited to the components of the middle lamella and primary cell wall, preserving the integrity of the cellulose microfibril structure within the cell walls. In order to protect the most sensitive components of the middle lamella and primary cell wall, additional protection (e.g. pre-treatment or impregnation) of the fibres might be necessary.

3.3. Properties of TRCMs

Fig. 8 shows the experimental force-deflection (F/δ) curves of the matrix control samples (red curves) and their associated TRCMs (blue curves) under three-point bending load for (a) PC, (c) 20% MK and (d) 30% MK, respectively. The curves of control and TRCM PC samples obtained from FE simulations are presented in Fig. 8b. Similar loading behavior was observed for different TRCM compositions during experimental testing and can be distinguished as follows: (1) initial phase with a nonlinear F/δ response caused by contact between the crosshead and tested specimens containing a certain degree of surface roughness (especially visible in 20% MK control samples), which explains the substantial difference in deflection values between experimental and numerical data of PC samples (surface roughness was not considered in FE simulations); (2) a linear elastic phase in which force increased rapidly within a range of small deflection, resulting in the appearance of the first matrix crack; and (3) crack propagation phase in which strain-hardening behavior, caused by the fibres' ability to bridge over and arrest the forming cracks, was observed. The third phase eventually ended due to a gradual crack width increase, which ultimately caused inefficient stress transfer from matrix to the fibres and gradual fibre-matrix interface weakening.

The flax textile reinforcement highly improved the ductility of the different cement-based matrices as seen from the greater area under the F/δ curve. The PC samples exhibited less ductile behavior when compared to those containing MK as seen from the lower stress values and deflection at the end of the crack propagation phase (observed from the appearance of the last peak, i.e., crack), after which textile reinforcement became inefficient in further crack arresting and matrix-fibre stress transfer.

FE analysis showed that TRCM can be modeled using the microplane model for the matrix, and the hyperelastic or linear isotropic material model for a textile layer. The simulated F/δ curves of PC samples (Fig. 8b) show that TRCM had lower stiffness than the control matrix, which is in agreement with experimental data; stiffness with respect to simulated PC TRCM was 84%, 79%, and 95% for hyperelastic, linear elastic without pre-stress and linear elastic with pre-stress model, respectively. FE model of TRCM showed 7% and 2% lower F_{max} (i.e., F_c of physical samples) for hyperelastic and linear elastic model without pre-stress when compared to simulated control sample. This pattern was found also in the experiments where the decrease is greater (on average, 37%, 11% and 25% for PC, 20% MK and 30% MK, respectively). The reason for the strength decrease of TRCM is that the cross-section of matrix in the FE model is weakened by textile layers to a certain degree, so matrix layers reach failure at lower global force due to stress concentrators (Fig. 9). The TRCM with linear elastic model with pre-stress did not exhibit failure as other models, but exhibited a certain strain hardening after reaching yield point since the textile layers provided their stiffness after the failure of the matrix.

FE models do not contain any irregularities at the specimen surfaces, so F/δ curves do not show any initial nonlinear phase as seen in experiments. This explains that the deflection at F_{max} is substantially lower than in experiments, even though reached F_{max} is within the statistical ranges of experiments. The FE model does not include debonding between textile and matrix as it was observed in physical experiments, which is why the simulated F/δ response cannot contain the typical “tooth-like” behavior for higher deflections, and the decrease of simulated F_{max} is lower than in reality. Linear isotropic model confirms that

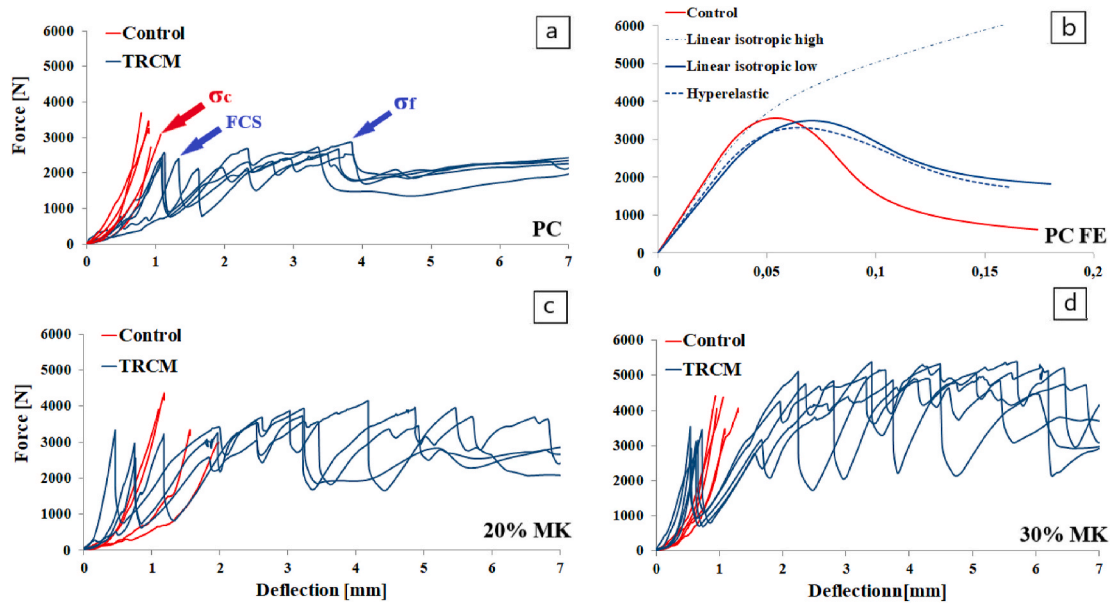


Fig. 8. Three-point bending force-deflection curves for control and TRCM samples with (a) PC matrix (experimental), (b) PC matrix (FE numerical data) c) 20% MK matrix (experimental data) and d) 30% MK (experimental data). * σ_c , FCS and σ_f stand for compressive strength of the control samples, first crack stress and flexural strength of TRCM samples, respectively. (color online only). (For interpretation of the references to color in this figure legend, the reader is referred to the Web version of this article.)

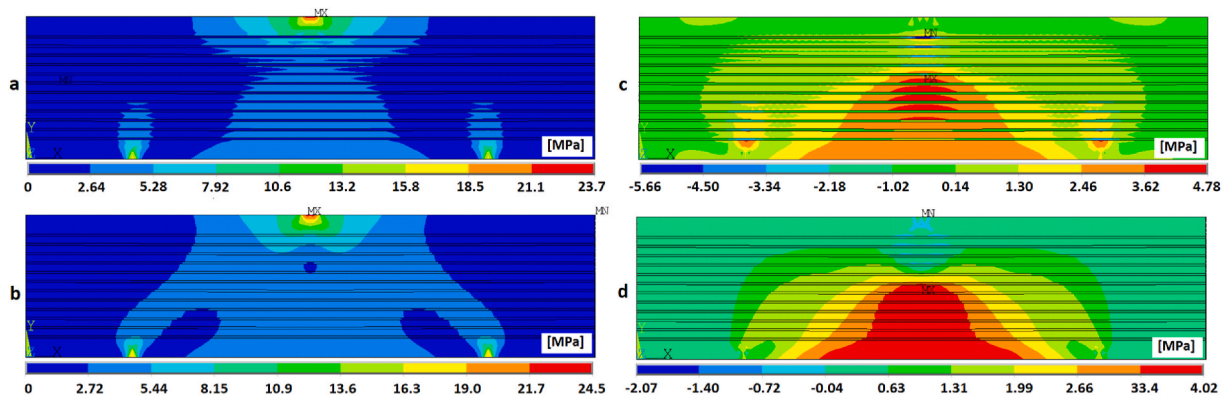


Fig. 9. (a, b) Von Mises stress and (c, d) 1st principal stress of the control (bottom) and TRCM (top) samples obtained from FE analysis at maximal force. (color online only). (For interpretation of the references to color in this figure legend, the reader is referred to the Web version of this article.)

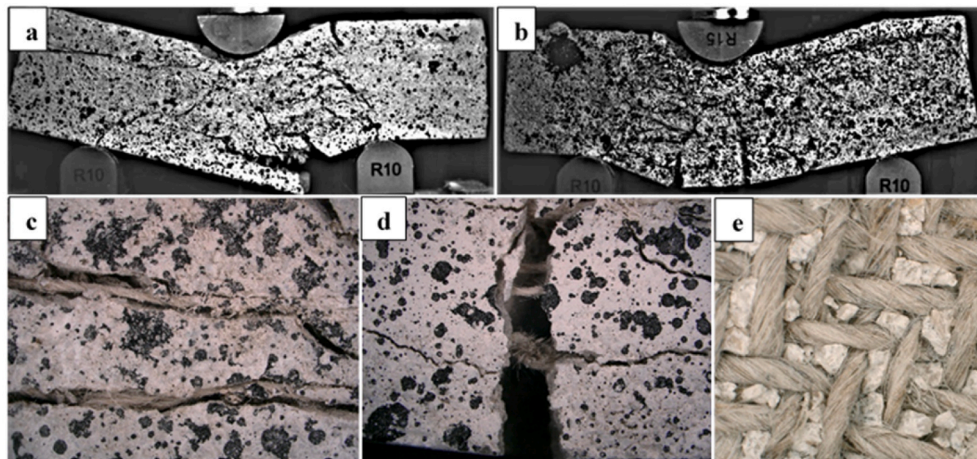


Fig. 10. Digital camera and digital microscope images showing cracking and failure mechanisms of (a, b) PC and (c, d and e) MK 30% samples. (color online only). (For interpretation of the references to color in this figure legend, the reader is referred to the Web version of this article.)

the textile layers would start participating in stiffness of the specimen at earlier stages of loading if they were pre-stressed in tension. In this study, the textile layers were inserted without pre-stress into the physical specimens. Thus they started significantly participating on F/δ response at higher deflection of the specimens, generating an effective strain-hardening. Because the FE model does not assume a pre-stress of the textile layers for hyperelastic and linear isotropic with low elastic modulus models, it shows a substantial decrease of stress values beyond reaching F_{max} for TRCM, as opposed to experimental data, where stress values continued to rise after the occurrence of the first crack. Furthermore, the linear isotropic model with high elastic modulus of textile (simulating pre-stress) should not be used for predicting F_{max} when the debonding between textile and matrix layers is not taken into account, as this is the case in the present study, which demonstrates the limitation of developed FE models and further research direction.

Fig. 10 shows cracking and failure mechanisms of PC (a and b) and 30% MK (c and d) samples at the end of the crack propagation phase. Fig. 10a shows that failure of the PC TRCM sample occurred mainly due to the delamination of the lower layer of matrix from the textile. The poor compaction of the PC matrix, highlighted in section 3.1, prevented its efficient penetration through the dense mesh openings of the textile, resulting in an inability of the PC matrix layers positioned between the textile reinforcement layer to connect, and hence providing a suboptimal fibre-matrix interface bond (Fig. 10c). This poor compaction is partly caused by limited ability of the fine aggregates (grain size of 0–1 mm) to penetrate the mesh openings of the textile (~0.6 mm). Textile reinforcement of 30% MK TRCM samples efficiently arrested the forming cracks (Fig. 10b and d), resulting in an enhanced ductile behavior when compared to the PC TRCM samples. Due to its high specific surface area, MK modified the microstructure of the matrix, ensuring better compaction and penetration through the textile layers, resulting in fewer void spaces around yarns and warp/weft junction points and creating a tighter interface bond (Fig. 10e). Additionally, the lower degree of fibre mineralization and better preservation of the fibres embedded in the 30% MK matrix, highlighted by TGA, contributed to the efficient crack arresting and fibre-matrix stress transfer. The crack propagation phase eventually ended due to a progressive increase in deflection and, therefore, cracks widths, ultimately causing fibre rupture (Fig. 10d).

Fig. 11 presents first crack stress (FCS) and flexural strength of control (σ_{Fc}) and TRCM (σ_{Ftrcm}) samples for different matrix compositions. The first crack stress of TRCM is lower than their flexural strength in all cases. This can be explained by the increased occurrence of defects (i.e., voids) caused by less efficient compaction of TRCM samples due to the presence of textile. A similar observation was reported by Peled et al. [42] for concrete matrix reinforced with different types of synthetic fabrics. These authors observed lower first crack stress for materials reinforced with higher yarn density (yarn/cm) textiles.

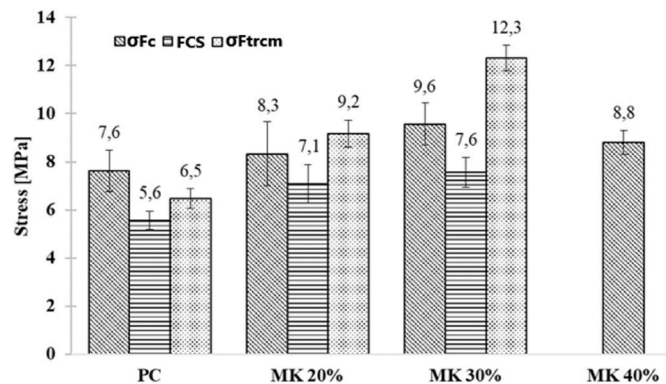


Fig. 11. Effect of MK content on first crack stress (FCS) and flexural strength of control (σ_{Fc}) and TRCM (σ_{Ftrcm}) samples.

High-density textiles, such as the one used in this study (10 yarn/cm), are associated with good mechanical anchorage ability due to a higher number of warp and weft junction points, and thus, good interfacial bond strength. However, the ability of the matrix to penetrate through the dense textile mesh is hindered, resulting in more voids between textile mesh openings, which weaken the matrix. When compared to PC TRCM samples, first crack stress of 20% and 30% MK samples increased by ~26.8% and 35.7%, respectively, due to the reduced porosity and, thus, increased compaction of samples containing MK. However, ANOVA revealed that MK 20% and MK 30% ($p = 0.502$) TRCM samples did not statistically differ in terms of first crack stress ($p < 0.01$), indicating there was no further increase in compaction past 20% MK.

For 20% and 30% MK content, the TRCM flexural strength was increased by 41.5% and 89.2%, respectively, when compared to the PC TRCM samples. ANOVA revealed that all the reinforced matrices statistically differ in terms of flexural strength (i.e., all possible group combinations had $p < 0.007$). This significant increase in strength can be attributed to several mechanisms. First, fibres' resistance to degradation increased with the addition of MK, resulting in total consumption of CH and much less fibre fracture and overall embrittlement, which contributed to the overall performance of the textile reinforcement and, thus, improved the ductility of the composite. Second, while the presence of high-density textile reinforcement in the sample diminishes the compaction and overall matrix quality, and therefore reduces the first crack stress, the efficient mechanical anchorage of the textile in the matrix governs the crack propagation phase, resulting in a strain-hardening behavior along with a substantial increase in flexural strength, especially when combined with a matrix-densening MK effect.

Fig. 12 shows the mechanical work of control (MW_c) and TRCM (MW_{trcm}) samples that represents the energy needed to deform the specimen to a certain deflection. The addition of MK does not lead to any statistical differences in mechanical work of control samples as examined by ANOVA ($p > 0.15$). On the contrary, all the matrices consisting of reinforced samples were statistically different from each other (i.e., all group combinations had $p < 0.0002$). As previously established, due to the poor adhesion between the matrix and textile reinforcement caused by weaker i.e., more brittle fibres and inefficient compaction between matrix and textile layers, PC TRCM samples had less ductile behavior when compared to samples of matrices containing MK. Stronger fibre-matrix interfacial bond, achieved by a reduction in CH content (i.e., alkalinity), and thus fibre degradation, and porosity of the matrices containing MK, allowed fibres to bridge over and arrest forming cracks as well as transfer stress from matrix to fibres more efficiently, which ultimately resulted in the material's capability to withstand higher loads over longer periods, and thus, achieve improvements in its ductile behavior. As with flexural strength, the 30% MK TRCM samples showed the best performance; on average, they absorbed 94.8% more mechanical work when compared to the TRCM PC samples.

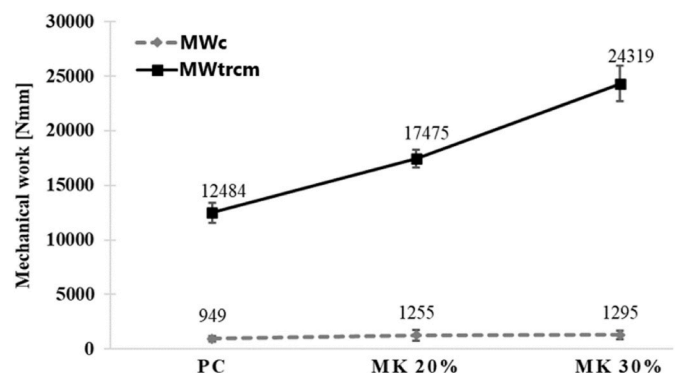


Fig. 12. Mechanical work of control (MW_c) and TRCM (MW_{trcm}) samples.

4. Conclusions

This study compared the overall performance of flax TRCMs produced using PC matrices and matrices containing 20–40% MK. The unreinforced matrix samples containing MK (up to 30%) displayed increased mechanical properties when compared to PC, and their phase composition analysis revealed the absence of CH, which contributed to preserving the strength and flexibility of the reinforcing flax fibres by limiting degradation of cellulose. However, degradation of other fibre components (primarily hemicellulose) was still present within all developed matrices. Pre-treatment or modification of the fibres would possibly prevent the degradation which occurs in the initial phase of cement hydration, and thus further research is proposed on the topic. The lower compaction within TRCM induced by the textile reinforcement was partially negated thanks to the MK's filler effect. The compaction of the samples could be further enhanced by improving the production process of TRCMs (i.e., automated instead of manual) and by using textiles with higher areal weight, which would reduce the volume of reinforcement needed to achieve desirable performance. While PC TRCM samples showed poor fibre-matrix interface bond, TRCM samples containing MK showed a good penetration of the matrix through the dense mesh openings of the textile, significantly contributing to the fibre-matrix interface bond and, hence, allowing efficient stress transfer from matrix to the fibres as well as fibres bridging over cracks. The improved durability of flax fibres and interface bond of TRCMs containing MK also resulted in a more ductile behavior, which in turn, resulted in improvements in flexural strength and mechanical work (i.e., energy absorption) when compared to the PC TRCMs. FE models were able to predict F_{max} with sufficient agreement with respect to the experimental results. Because FE models included only damage principles for matrix and no debonding, they could not predict post-failure tooth-like behavior and hardening as observed experimentally. The textile layers may be modeled either as hyperelastic or linear elastic materials, both having a similar effect on F_{max} and stiffness. Future FE models should focus on a definition of debonding between matrix and textile reinforcement in order to take all phases of the F/δ response into account.

Funding

The authors gratefully acknowledge the European Commission for funding the InnoRenew project [H2020 WIDESPREAD-2-Teaming grant number 739574] and the Republic of Slovenia [investment funding from the Republic of Slovenia and the European Regional Development Fund], Horizon 2020, the EU Framework Programme for Research and Innovation [Marie Skłodowska-Curie Actions grant number 898179], Cost Action CA17107, which initiated this research in the frame of a short-term scientific mission and Slovenian Research Agency (research core funding No. P2-0273).

Declaration of competing interest

The authors declare that they have no known competing financial interests or personal relationships that could have appeared to influence the work reported in this paper.

References

- [1] 'Cement – Analysis', IEA. <https://iea.org/reports/cement> (accessed Mar. 26, 2021).
- [2] O. Onuaguluchi, N. Banthia, Plant-based natural fibre reinforced cement composites: a review, *Cement Concr. Compos.* 68 (Apr. 2016) 96–108, <https://doi.org/10.1016/j.cemconcomp.2016.02.014>.
- [3] M. Ardanuy, J. Claramunt, R.D. Toledo Filho, Cellulosic fiber reinforced cement-based composites: a review of recent research, *Construct. Build. Mater.* 79 (Mar. 2015) 115–128, <https://doi.org/10.1016/j.conbuildmat.2015.01.035>.
- [4] O. Faruk, A.K. Bledzki, H.-P. Fink, M. Sain, Biocomposites reinforced with natural fibers: 2000–2010, *Prog. Polym. Sci.* 37 (11) (Nov. 2012) 1552–1596, <https://doi.org/10.1016/j.progpolymsci.2012.04.003>.
- [5] L. Ferrara, S.R. Ferreira, V. Krelani, P. Lima, F. Silva, R.D.T. Filho, Cementitious composites reinforced with natural fibres, *Recent Adv. Green Concr. Struct. Purp. Contrib. EU-FP7 Proj. EnCoRe* (2017) 197–331, https://doi.org/10.1007/978-3-319-56797-6_9.
- [6] R. Olivito, O.A. Cevallos, A. Carrozzini, Development of durable cementitious composites using sisal and flax fabrics for reinforcement of masonry structures, *Mater. Des.* 57 (2014) 256–258, <https://doi.org/10.1016/j.matdes.2013.11.023>.
- [7] L. Yan, K. Jayaraman, Flax fibre and its composites - a review, *Compos. B Eng.* 56 (Aug. 2013) 296–317, <https://doi.org/10.1016/j.compositesb.2013.08.014>.
- [8] D. Asprone, M. Durante, A. Prota, G. Manfredi, Potential of structural pozzolanic matrix-hemp fiber grid composites, *Constr. Build. Mater. - CONSTR BUILD MATER* 25 (Jun. 2011) 2867–2874, <https://doi.org/10.1016/j.conbuildmat.2010.12.046>.
- [9] L. Ferrara, S.R. Ferreira, V. Krelani, P. Lima, F. Silva, R.D.T. Filho, Cementitious composites reinforced with natural fibres, in: J.A.O. Barros, L. Ferrara, E. Martinelli (Eds.), *Recent Advances on Green Concrete for Structural Purposes: the Contribution of the EU-FP7 Project EnCoRe*, Springer International Publishing, Cham, 2017, pp. 197–331, https://doi.org/10.1007/978-3-319-56797-6_9.
- [10] R. Olivito, O. Cevallos, A. Carrozzini, Development of durable cementitious composites using sisal and flax fabrics for reinforcement of masonry structures, *Mater. Des.* 57 (May 2014) 258–268, <https://doi.org/10.1016/j.matdes.2013.11.023>.
- [11] D. Asprone, M. Durante, A. Prota, G. Manfredi, Potential of structural pozzolanic matrix-hemp fiber grid composites, *Construct. Build. Mater.* 25 (6) (Jun. 2011) 2867–2874, <https://doi.org/10.1016/j.conbuildmat.2010.12.046>.
- [12] M.A. Aziz, P. Paramasivam, S.L. Lee, Prospects for natural fibre reinforced concretes in construction, *Int. J. Cem. Compos. Lightweight Concr.* 3 (2) (May 1981) 123–132, [https://doi.org/10.1016/0262-5075\(81\)90006-3](https://doi.org/10.1016/0262-5075(81)90006-3).
- [13] B.J. Mohr, H. Nanko, K.E. Kurtis, Durability of kraft pulp fiber-cement composites to wet/dry cycling, *Cement Concr. Compos.* 27 (4) (Apr. 2005) 435–448, <https://doi.org/10.1016/j.cemconcomp.2004.07.006>.
- [14] M. Ardanuy, J. Claramunt, J. Garcia-Hortal, M. Barra Bizinotto, Fiber-matrix interactions in cement mortar composites reinforced with cellulosic fibers, *Cellulose* 18 (Apr. 2011) 281–289, <https://doi.org/10.1007/s10570-011-9493-3>.
- [15] A. Peled, B. Mobasher, 'Pultruded fabric-cement composites', *Mater. J.* 102 (1) (Jan. 2005) 15–23, <https://doi.org/10.14359/14245>.
- [16] A. Peled, A. Bentur, Fabric structure and its reinforcing efficiency in textile reinforced cement composites, *Compos. Part Appl. Sci. Manuf.* 34 (2) (Feb. 2003) 107–118, [https://doi.org/10.1016/S1359-835X\(03\)00003-4](https://doi.org/10.1016/S1359-835X(03)00003-4).
- [17] O.A. Cevallos, R.S. Olivito, Effects of fabric parameters on the tensile behaviour of sustainable cementitious composites, *Compos. B Eng.* 69 (Feb. 2015) 256–266, <https://doi.org/10.1016/j.compositesb.2014.10.004>.
- [18] O. Cevallos, R. Olivito, Effects of fabric parameters on the tensile behaviour of sustainable cementitious composites, *Compos. B Eng.* 69 (Oct. 2014), <https://doi.org/10.1016/j.compositesb.2014.10.004>.
- [19] N. Trochoutsou, M. Di Benedetto, K. Pilakoutas, M. Guadagnini, Mechanical characterisation of flax and jute textile-reinforced mortars, *Construct. Build. Mater.* 271 (Feb. 2021) 121564, <https://doi.org/10.1016/j.conbuildmat.2020.121564>.
- [20] D. Snoeck, N. De Belie, Mechanical and self-healing properties of cementitious composites reinforced with flax and cottonised flax, and compared with polyvinyl alcohol fibres, *Biosyst. Eng.* 111 (4) (Apr. 2012) 325–335, <https://doi.org/10.1016/j.biosystemseng.2011.12.005>.
- [21] G. Ferrara, B. Coppola, L. Di Maio, L. Incarnato, E. Martinelli, Tensile strength of flax fabrics to be used as reinforcement in cement-based composites: experimental tests under different environmental exposures, *Compos. B Eng.* 168 (Jul. 2019) 511–523, <https://doi.org/10.1016/j.compositesb.2019.03.062>.
- [22] L. Mercedes, L. Gil, E. Bernat-Maso, Mechanical performance of vegetal fabric reinforced cementitious matrix (FRMC) composites, *Construct. Build. Mater.* 175 (Jun. 2018) 161–173, <https://doi.org/10.1016/j.conbuildmat.2018.04.171>.
- [23] M.E.A. Fidelis, R.D. Toledo Filho, F. de A. Silva, V. Mechtcherine, M. Butler, S. Hempel, The effect of accelerated aging on the interface of jute textile reinforced concrete, *Cement Concr. Compos.* 74 (Nov. 2016) 7–15, <https://doi.org/10.1016/j.cemconcomp.2016.09.002>.
- [24] A. Hakamy, F.U.A. Shaikh, I.M. Low, Characteristics of hemp fabric reinforced nanoclay-cement nanocomposites, *Cement Concr. Compos.* 50 (Jul. 2014) 27–35, <https://doi.org/10.1016/j.cemconcomp.2014.03.002>.
- [25] M. Elmessiry, A.-B. Mito, A. Aloufy, E. El-Tahan, Effect of fabric material and tightness on the mechanical properties of fabric-cement composites, *Alex. Eng. J.* 53 (Dec. 2014), <https://doi.org/10.1016/j.aej.2014.09.002>.
- [26] L. Souza, L. Souza, F. Silva, Mechanics and cracking mechanisms in natural curauá textile reinforced concrete, in: *Strain-Hardening Cement-Based Composites. SHCC 2017. RILEM Bookseries*, vol. 15, 2017, pp. 359–366, https://doi.org/10.1007/978-94-024-1194-2_42.
- [27] A. Bourmaud, J. Beaugrand, D.U. Shah, V. Placet, C. Baley, Towards the design of high-performance plant fibre composites, *Prog. Mater. Sci.* 97 (Aug. 2018) 347–408, <https://doi.org/10.1016/j.pmatsci.2018.05.005>.
- [28] K.L. Pickering, M.G.A. Efendy, T.M. Le, A review of recent developments in natural fibre composites and their mechanical performance, *Compos. Part Appl. Sci. Manuf.* 83 (Apr. 2016) 98–112, <https://doi.org/10.1016/j.compositesa.2015.08.038>.
- [29] G. Ferrara, M. Pepe, E. Martinelli, R.D. Toledo Filho, Tensile behavior of flax textile reinforced lime-mortar: influence of reinforcement amount and textile impregnation, *Cement Concr. Compos.* 119 (May 2021) 103984, <https://doi.org/10.1016/j.cemconcomp.2021.103984>.
- [30] G. Ferrara, M. Pepe, R.D. Toledo Filho, E. Martinelli, Mechanical response and analysis of cracking process in hybrid TRM composites with flax textile and curauá fibres, *Polymers* 13 (5) (Jan. 2021) 5, <https://doi.org/10.3390/polym13050715>.

- [31] H.H. Bache, G.M. Idorn, P. Nepper-christensen, J. Neilsen, Morphology OF calcium hydroxide IN cement paste, Highw. Res. Board Spec. Rep. (90) (1966). <https://trid.trb.org/view/101450>. (Accessed 8 November 2021).
- [32] H.-E. Gram, *Durability of Natural Fibres in Concrete*, Swedish Cement and Concrete Research Institute, 1983. Stockholm: Cement- och betonginst.
- [33] R. Toledo Filho, K. Scrivener, G. England, K. Ghavami, Durability of alkali-sensitive sisal and coconut fibres in cement mortar composites, *Cement Concr. Compos.* 22 (Apr. 2000) 127–143, [https://doi.org/10.1016/S0958-9465\(99\)00039-6](https://doi.org/10.1016/S0958-9465(99)00039-6).
- [34] R.D. Toledo Filho, F. de A. Silva, E.M.R. Fairbairn, J. de A.M. Filho, Durability of compression molded sisal fiber reinforced mortar laminates, *Construct. Build. Mater.* 23 (6) (Jun. 2009) 2409–2420, <https://doi.org/10.1016/j.conbuildmat.2008.10.012>.
- [35] A. Ali, et al., Hydrophobic treatment of natural fibers and their composites – a review, *J. Ind. Textil.* 47 (May 2016), <https://doi.org/10.1177/1528083716654468>.
- [36] M.F. Canovas, N.H. Selva, G.M. Kawiche, New economical solutions for improvement of durability of Portland cement mortars reinforced with sisal fibres, *Mater. Struct.* 25 (7) (Aug. 1992) 417–422, <https://doi.org/10.1007/BF02472258>.
- [37] R.D. Toledo Filho, K. Ghavami, G.L. England, K. Scrivener, Development of vegetable fibre–mortar composites of improved durability, *Cement Concr. Compos.* 25 (2) (Feb. 2003) 185–196, [https://doi.org/10.1016/S0958-9465\(02\)00018-5](https://doi.org/10.1016/S0958-9465(02)00018-5).
- [38] Z. Berhane, Performance of natural fibre reinforced mortar roofing tiles, *Mater. Struct.* 27 (6) (Jul. 1994) 347–352, <https://doi.org/10.1007/BF02473427>.
- [39] M. Glavind, 5 - sustainability of cement, concrete and cement replacement materials in construction, in: J.M. Khatib (Ed.), *Sustainability of Construction Materials*, Woodhead Publishing, 2009, pp. 120–147, <https://doi.org/10.1533/9781845695842.120>.
- [40] P. Duan, Z. Shui, W. Chen, C. Shen, Effects of metakaolin, silica fume and slag on pore structure, interfacial transition zone and compressive strength of concrete, *Construct. Build. Mater.* 44 (Jul. 2013) 1–6, <https://doi.org/10.1016/j.conbuildmat.2013.02.075>.
- [41] Y. Wei, W. Yao, X. Xing, M. Wu, Quantitative evaluation of hydrated cement modified by silica fume using QXRD, 27Al MAS NMR, TG–DSC and selective dissolution techniques, *Construct. Build. Mater.* 36 (Nov. 2012) 925–932, <https://doi.org/10.1016/j.conbuildmat.2012.06.075>.
- [42] A. Peled, A. Bentur, D. Yankelevsky, Flexural performance of cementitious composites reinforced with woven fabrics, *J. Mater. Civ. Eng.* 11 (4) (Nov. 1999) 325–330, [10.1061/\(ASCE\)0899-1561\(1999\)11:4\(325\)](https://doi.org/10.1061/(ASCE)0899-1561(1999)11:4(325)).
- [43] G.L. Thankam, N.T. Renganathan, Ideal supplementary cementing material – metakaolin: A review, *Int. Rev. Appl. Sci. Eng.* 11 (1) (Apr. 2020) 58–65, <https://doi.org/10.1556/1848.2020.00008>.
- [44] R. Snellings, X-ray powder diffraction applied to cement, in: *A Practical Guide to Microstructural Analysis of Cementitious Materials*, first ed., CRC Press., Boca Raton, 2015, pp. 107–176, <https://doi.org/10.1201/b19074-5>.
- [45] T. Kim, J. Olek, Effects of sample preparation and interpretation of thermogravimetric curves on calcium hydroxide in hydrated pastes and mortars, *Transport. Res. Rec.* 2290 (1) (Jan. 2012) 10–18, <https://doi.org/10.3141/2290-02>.
- [46] S. Wild, J.M. Khatib, Portlandite consumption in metakaolin cement pastes and mortars, *Cement Concr. Res.* 27 (1) (Jan. 1997) 137–146, [https://doi.org/10.1016/S0008-8846\(96\)00187-1](https://doi.org/10.1016/S0008-8846(96)00187-1).
- [47] S. Wild, J.M. Khatib, A. Jones, Relative strength, pozzolanic activity and cement hydration in superplasticised metakaolin concrete, *Cement Concr. Res.* 26 (10) (Oct. 1996) 1537–1544, [https://doi.org/10.1016/0008-8846\(96\)00148-2](https://doi.org/10.1016/0008-8846(96)00148-2).
- [48] B. El-Jazairi, J.M. Illston, A simultaneous semi-isothermal method of thermogravimetry and derivative thermogravimetry, and its application to cement pastes, *Cement Concr. Res.* 7 (3) (May 1977) 247–257, [https://doi.org/10.1016/0008-8846\(77\)90086-2](https://doi.org/10.1016/0008-8846(77)90086-2).
- [49] K. Scrivener, R. Snellings, B. Lothenbach, *A Practical Guide to Microstructural Analysis of Cementitious Materials*, CRC Press, 2018.
- [50] I. Zreid, M. Kaliske, An implicit gradient formulation for microplane Drucker-Prager plasticity, *Int. J. Plast.* 83 (Aug. 2016) 252–272, <https://doi.org/10.1016/j.ijplas.2016.04.013>.
- [51] American Concrete Institute, *Building Code Requirements for Structural Concrete (ACI 318-08) and Commentary: an ACI Standard*, American Concrete Institute, Farmington Hills, MI, 2008.
- [52] M.E.A. Fidelis, R.D. Toledo Filho, F. de A. Silva, V. Mechtcherine, M. Butler, S. Hempel, The effect of accelerated aging on the interface of jute textile reinforced concrete, *Cement Concr. Compos.* 74 (Nov. 2016) 7–15, <https://doi.org/10.1016/j.cemconcomp.2016.09.002>.
- [53] I. Halikia, L. Zoumpoulakis, I. Christodoulou, D. Prattis, Kinetic study of the thermal decomposition of calcium carbonate by isothermal methods of analysis, *Eur. J. Miner. Process. Environ. Protect.* 1 (Jan. 2001).
- [54] M. Olszak-Humienik, M. Jablonski, Thermal behavior of natural dolomite, *J. Therm. Anal. Calorim.* 119 (Dec. 2014), <https://doi.org/10.1007/s10973-014-4301-6>.
- [55] B. Karimi Shahraki, B. Mehrabi, R. Dabiri, Thermal behavior of Zefreh dolomite mine (Central Iran), *J. Min. Metall. B Metall.* 45 (Jan. 2009), <https://doi.org/10.2298/JMMB0901035S>.
- [56] K.S.P. Karunadasa, C.H. Manoratne, H.M.T.G.A. Pitawala, R.M.G. Rajapakse, Thermal decomposition of calcium carbonate (calcite polymorph) as examined by in-situ high-temperature X-ray powder diffraction, *J. Phys. Chem. Solid.* 134 (Nov. 2019) 21–28, <https://doi.org/10.1016/j.jpcs.2019.05.023>.
- [57] R. Siddique, J. Klaus, Influence of metakaolin on the properties of mortar and concrete: a review, *Appl. Clay Sci.* 43 (3) (Mar. 2009) 392–400, <https://doi.org/10.1016/j.clay.2008.11.007>.
- [58] M. Aqel, D. Panesar, Physical and chemical effects of limestone filler on the hydration of steam cured cement paste and mortar, *Rev. ALCONPAT* 10 (Apr. 2020) 191–205, <https://doi.org/10.21041/ra.v10i2.481>.
- [59] C. Cherif, The textile process chain and classification of textile semi-finished products, in: C. Cherif (Ed.), *Textile Materials for Lightweight Constructions: Technologies - Methods - Materials - Properties*, Springer, Berlin, Heidelberg, 2016, pp. 9–35, https://doi.org/10.1007/978-3-662-46341-3_2.
- [60] H. Yang, R. Yan, H. Chen, D.H. Lee, C. Zheng, Characteristics of hemicellulose, cellulose and lignin pyrolysis, *Fuel* 86 (12) (Aug. 2007) 1781–1788, <https://doi.org/10.1016/j.fuel.2006.12.013>.
- [61] M. Frías, J. Cabrera, Pore size distribution and degree of hydration of metakaolin–cement pastes, *Cement Concr. Res.* 30 (Apr. 2000) 561–569, [https://doi.org/10.1016/S0008-8846\(00\)00203-9](https://doi.org/10.1016/S0008-8846(00)00203-9).
- [62] J. Wei, C. Meyer, Degradation mechanisms of natural fiber in the matrix of cement composites, *Cement Concr. Res.* 73 (Jul. 2015) 1–16, <https://doi.org/10.1016/j.cemconres.2015.02.019>.